Investigation of Nonlinear Thermo-Elastic Behavior of Fluid Conveying Piezoelectric Microtube Reinforced by Functionally Distributed Carbon Nanotubes on Viscoelastic-Hetenyi Foundation

Mehdi Azhdarzadeh[1], Reza Jahangiri[2,*], Akbar Allahverdizadeh[3], Behnam Dadashzadeh[3] and Ramin Nabati[2]

[1]*Department of Mechanical Engineering, University of Alberta, Edmonton, AB, Canada*
[2]*Department of Mechanical Engineering, Azad University, Salmas Branch, Salmas, Iran*
[3]*Department of Mechatronics Engineering, University of Tabriz, Tabriz, Iran*
E-mail: r_jahangiri@tabrizu.ac.ir
[*]*Corresponding Author*

Abstract

In this paper, nonlinear and nonlocal thermo-elastic behavior of a microtube reinforced by Functionally Distributed Carbon Nanotubes, with internal and external piezoelectric layers, in the presence of nonlinear viscoelastic-Hetenyi foundation, and axial fluid flow inside the microtube is studied. Nonlinear partial differential equations governing the system are derived using Reddy's third-order shear deformations theory along with the Von-Karman theory including the effect of fluid viscosity. Then, the equations are converted to time-dependent ordinary nonlinear equations using the Galerkin

method. Afterward, the governing equations of the microtube's lateral displacements are solved using the multiple scales method. The analysis of the piezoelectric's parametric resonance is performed by obtaining trivial and nontrivial stationary solutions and plotting characteristic curves of the frequency response and voltage response. At the end, the effect of different parameters including the flow velocity, excitation voltage, parameters of the foundation, viscosity parameter, thermal loading and nanotubes' volume fraction index on the nonlinear behavior of the system, under parametric resonance condition, is investigated.

Keywords: Microtube, piezoelectric, reinforced, viscoelastic foundation.

1 Introduction

Micro and nano-electromechanical systems are widely used as the active parts of accelerometers, gyroscopes, chemical sensors, and switches. Therefore, the study of the nonlinear behavior of microtubes reinforced with carbon nanotubes carrying fluid is receiving more attention [1–3]. Moreover, the application of micro/nanotubes has grown during the last recent decades in high-tech industries such as drug delivery applications, electrical board cooling, bio-sensors, and semiconductors [1, 4–6]. The interaction between fluid and solid on the boundaries and velocity profile are the keys in the nonlinear dynamic modeling of these problems [7], emphasizing the importance of such studies further.

[8, 9] studied theoretically and experimentally the dynamic instability of cantilever pipes carrying fluid in the first mode of vibration, and showed that the instability is a hoop instability. [10] performed a dynamic analysis on fluid conveying tubes and demonstrated that the mass of the fluid needs to be included in the modeling to have acceptable accuracy. [11–13] studied the linear and nonlinear vibration and dynamic instability of nano and microtubes conveying fluid. [14] developed a size-dependent beam model to study the nonlinear free vibration of functionally graded carbon nanobeams (FG-CNT). He utilized Hamilton's principle to derive the equations of motion.

Linear and nonlinear models of Winkler and Pasternak are used in most of the current studies on the dynamic behavior of fluid conveying tubes on elastic foundations, where the stiffness of the foundation is modeled by a linear spring having a uniform distribution of forces. [15] used the finite element method along with the linear Winkler foundation to analyze the effect

of elastic foundation on the dynamic behavior of the tubes and showed that an increase in the stiffness of the foundation will increase the natural frequency of the system and critical velocity of the fluid. [16] applied multiple scales method to the viscoelastic fluid conveying tubes and investigated the condition of dynamic stability including different parameters and showed that at high fluid velocities, the system experiences flutter instability. [17] included the effect of initial imperfection in the stability analysis of the nano-pipes. They modeled the FG-CNT as an Euler-Bernouli beam. [7] investigated the nonlinear free and forced vibration of the tubes on a nonlinear elastic foundation using a modified power-law function, including the effect of porosity as imperfection. [18] looked into the flow-induced vibration on the fatigue life of the FG-CNTs. [19] explored the nonlinear vibration of fluid-conveying cantilevered pipe under the action of an axial base excitation, considering both 2D and 3D effects. [20] used a quasi-zero stiffness system to model the vibration of the fluid-conveying pipe with two nonlinear isolators.

[21] used differential quadratic method to discretize the governing equations of fluid conveying nanotubes, and by involving the effect of coupled modes proved that at higher velocities of fluid flow flutter instability occurs. [22] investigated the problem of vibration and instability of single-walled carbon fluid conveying nanotubes. He used the nonlocal elasticity theory and noticed that the natural frequency of the system is decreased by an increase in the nonlocal shear parameter. He also found that an increase in the elasticity parameters increases the natural frequency and critical velocities corresponding to the flutter instability. [23] studied nonlinear dynamic instability of composite piezoelectric plates reinforced with nanotubes having geometrical deficiencies. Their research was focused on the effects of parameters such as excitation voltage and distribution pattern of nanotubes on the parametric resonance of the plates.

To investigate the effect of longitudinal piezoelectric excitation on the vibration of fluid conveying carbon nanotubes, [24] analyzed the stability and nonlinear vibration of nanotubes using Winkler elastic foundation and demonstrated that the foundation's effect is not negligible. [25] conducted an electro-thermo-mechanical study on the nonlinear dynamic response of reinforced cylindrical piezoelectric shells and showed that the amplitude of excitation voltage is the main parameter governing the response. [26] used elasticity theory to investigate the free vibration of the cylindrical piezoelectric panel that is reinforced with nanotubes under simply supported boundary condition, and illustrated the effects of volumetric fraction index, their distribution pattern, the thickness of the piezoelectric layer, and dimension

ratios on the behavior of the system. [27, 28] employed the modified couple stress and Timoshenko beam theory to investigate the problem of buckling and nonlocal vibration of functionally graded piezoelectric nanoplate and demonstrated the effects of dimensions, nonlocal stress parameter, volumetric fraction index, and coefficients of Winkler and Pasternak foundation on the natural frequency.

Past studies have not investigated the effect of the nonlinear Hetenyi foundation on the nonlinear and nonlocal behavior of sandwiched piezo-electric fluid conveying microtubes reinforced with carbon nanotubes using Reddy's third-order shear deformations theory and Eringen's nonlocal model under parametric resonance conditions. In the current research, this problem is studied for the piezoelectric microtubes with a FG-X nanotube pattern of reinforcement. FG-X pattern is one of the most common patterns that results in a higher critical load [29]. The slip boundary condition is assumed for the fluid and governing equations of axial, rotational, and radial motion are derived. Afterward, the effect of different parameters on the nonlinear behavior of the system under parametric excitation of the piezoelectric, at flow velocities lower than flutter instability, and under parametric resonance is studied.

2 Modeling Single-Walled Microtubes Reinforced with Carbon Nanotubes

Nanotubes with a large Young modulus have high tensile strength and can be used to reinforce composites. Figure 1 depicts a schematic of a fluid conveying microtube reinforced with nanotubes.

The slip condition is assumed for the flow on the inner wall surface of the tube, and both ends of the tube are assumed to have a simply supported boundary condition. V_f is the Flow velocity through the axial direction of the tube and the piezoelectric microtube is excited in the radial direction on a nonlinear Hetenyi foundation.

Hetenyi foundation is assumed to have a continuous structure while keeping its contact with the tube during the deformation during the large deformation.

As can be seen in Figure 2 the tube has a length of L, radius R, tube thickness h and piezoelectric thickness of h_p. The cross-sectional area of the micro tube and the cross-sectional area of the fluid conveying section is approximated to be $A_b = 2\pi R(h + 2h_p)$ and $A_f = \pi(R - h/2 - h_p)^2$.
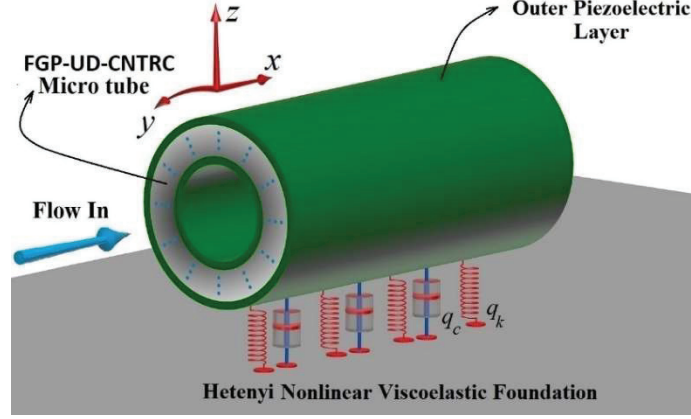
Figure 1 Fluid conveying microtube on a Hetenyi foundation under piezoelectric excitation.

The volume fraction index of the nanotubes, using the rule of mixtures, can be written as [27]

$$V_{CNT} = w(z)V_{CNT}^*$$

$$V_{CNT}^* = \frac{w_{CNT}}{w_{CNT} + \rho_{CNT}/\rho_m(1 - w_{CNT})}$$

$$V_f + V_m = 1 \tag{1}$$

where m and f subscripts denote matrix and reinforcing agent, respectively. The equation above is based on a linear variation of the volume fraction of nanotubes in the thickness direction. Here V_{CNT}, w_{CNT} and ρ_{CNT} are the volume fraction, mass fraction, and density of the carbon nanotubes and $w(z) = 1$ is corresponding to the uniform distribution along the thickness direction.

The volume fraction for the FG-X pattern, Figure 2, is

$$V_{CNT}(z) = 2\left(\frac{2|z|}{h}\right)V_{CNT}^* \quad \text{(FG-X CNTRC)} \tag{2}$$

Using the Equations (1) and (2), Young modulus along the axial direction and effective shear modulus of the composite tube can be written as
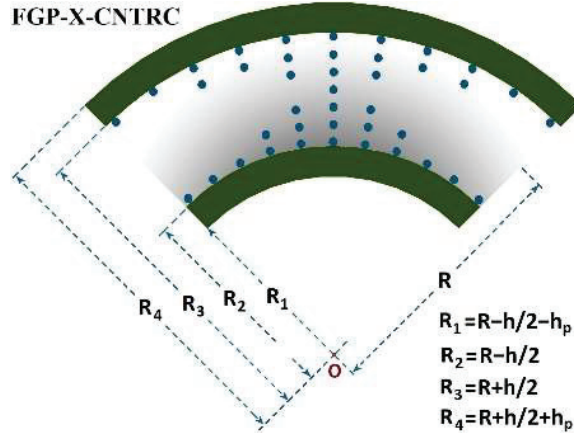
$$E_{11} = \eta_1 V_{CNT} E_{11}^{CNT} + V_m E_m$$

Figure 2   FG-X pattern for carbon nanotubes in the microtube.

$$\frac{\eta_2}{E_{22}} = \frac{V_{CNT}}{E_{22}^{CNT}} + \frac{V_m}{E_m}$$

$$\frac{\eta_3}{G_{12}} = \frac{V_{CNT}}{G_{12}^{CNT}} + \frac{V_m}{G_m} \tag{3}$$

Here E_{11}^{CNT} and E_{22}^{CNT} are Young's modulus and G_{12}^{CNT} is the shear modulus of the nanotubes. E_m and G_m are the properties related to the matrix and η_i, $i = 1, 2, 3$, is the efficiency parameter and Poisson's ratio in the thickness direction is

$$v_{12} = V_{CNT}^* v_{12}^{CNT} + V_m v_m \tag{4}$$

The following nonlinear equation shows the relation between the force and displacement of the viscoelastic foundation [24].

$$q_e(x,t) = K_1 w(x,t) - K_2 \frac{\partial^4 w(x,t)}{\partial^4 x} + K_3 w(x,t)^3 + C_v \dot{w}(x,t) \tag{5}$$

where q_e is the force per unit area and $w(x,t)$ indicates the deflection of the microtube. Here, $w(x,t)$ shows the displacement of the points on the microtube in the lateral direction and q_e is the applied force along the contact line over a unit length of the tube.

Parameters $K_1 = k_w$ and $K_3 = k_{nl}$ are the linear stiffness and nonlinear Winkler foundation parameters and $K_2 = k_h$ is the shear layer stiffness of the Hetenyi foundation. C_v is the damping coefficient of the foundation.

Using the shear deformation theory, the displacement field in the x and z direction for the inner points of the beam can be expressed as [30]

$$U(x, z, t) = u(x, t) + z\phi_x(x, t) - c_1 z^3 \phi_x(x, t) - c_1 z^3 \frac{\partial w(x, t)}{\partial x}$$

$$W(x, z, t) = w(x, t) \tag{6}$$

where $c_1 = \frac{4}{3h^2}$, $c_2 = 3c_1$ and ϕ_x are representing the rotation of the vector perpendicular to the cross-sectional area of the microtube. From the Reddy's third-order shear deformation theory, the relation between strain and displacement is rewritten as

$$\boldsymbol{\varepsilon_{xx} = u_{,x} + 1/2(w_{,x})^2 + z\phi_{x,x} - c_1 z^3 (w_{,xx} + \phi_{x,x})} \tag{7}$$

Considering the effect of linear thermal gradient (variation) between the upper and lower surfaces of the core, the stress-strain relation of the piezoelectric microtubes in the thickness direction can be written as [28],

$$\sigma_{xx} = \begin{cases} E_{11}(z)\varepsilon_{xx} - e_{31}E_z, & R + \dfrac{h}{2} \leq z \leq R + \dfrac{h}{2} + h_p \\[2mm] E_{11}(z)(\varepsilon_{xx} - \varepsilon_{11}\Delta T), & R - \dfrac{h}{2} \leq z \leq R + \dfrac{h}{2} \\[2mm] E_{11}(z)\varepsilon_{xx} - e_{31}E_z, & R - \dfrac{h}{2} - h_p \leq z \leq R - \dfrac{h}{2} \end{cases} \tag{8}$$

In the equation above, E_z is the electrical field applied to the piezoelectric and e_{31} is the piezoelectric constant. In Equations (2–8), $E_{11}(z)$, the effective axial modulus, and α_{11}, the thermal expansion coefficient in the longitudinal direction of the CNTRC micro-tube, are

$$E_{11}^{FG\text{-}CNT}(z) = \eta_1 V_{CNT}(z) E_{11}^{CNT} + V_m(z) E_m$$

$$\alpha_{11} = \frac{V_{CNT}(z) E_{11}^{CNT} \alpha_{11}^{CNT} + V_m(z) E_m \alpha_m}{V_{CNT}(z) E_{11}^{CNT} + V_m(z) E_m} \tag{9}$$

Here E_{11}^{CNT} and E_m are the Young Modulus of the carbon nanotubes and matrix, and η_1 is the efficiency coefficient of the distribution pattern along the axial direction. Moreover, in Equation (8), α_{11}^{CNT} and α_m are the thermal expansion coefficients of the CNT and the matrix, respectively.

Due to the small thickness of the piezoelectric, the self-induced electric potential will be negligible compared to the external excitation voltage, which is applied to the piezoelectric in the thickness direction. According to the

above assumptions, the relation between the applied voltage and input electric field intensity can be written as,

$$E_z = \frac{V_p(t)}{h_p} \tag{10}$$

Applying the Reddy's third-order shear deformation theory, axial force, N_x, bending moment, M_x, and third-order bending moment, T_x, involving the thermal gradient and piezo-electric-related effects, can be derived by conducting an integration on the cross-sectional area of the microtube, as follows.

$$N_x = A_{11}\varepsilon_m + B_{11}\varepsilon_b + E_{11}\varepsilon_{hb} + N_x^{\text{Piezo}} - N_x^{\Delta T}$$

$$M_x = B_{11}\varepsilon_m + D_{11}\varepsilon_b + F_{11}\varepsilon_{hb} + M_x^{\text{Piezo}} - M_x^{\Delta T}$$

$$T_x = E_{11}\varepsilon_m + F_{11}\varepsilon_b + H_{11}\varepsilon_{hb} + T_x^{\text{Piezo}} - T_x^{\Delta T} \tag{11}$$

In the equation above A_{11}, B_{11} and D_{11} are the components of the matrix of axial stiffness, bending-axial coupling, and bending, respectively and E_{11}, F_{11} and H_{11} are the components of bending stiffness matrices for the microtube.

By performing a time integration over the cross-sectional area of the microtube for the strain energy stored and using the Green's theorem and dual integration over the cross-sectional area of the microtube, and linear integration over the circumference of this area, it reads,

$$\int_{t_1}^{t_2} \delta U dt = \int_{t_1}^{t_2} \int_0^L \int_{A_b} \sigma_x \delta \varepsilon_x dA dx dt$$

$$= \int_{t_1}^{t_2} \int_0^L \int_{A_b} \sigma_x \left(\frac{\partial(\delta u)}{\partial x} + \frac{\partial w}{\partial x}\frac{\partial(\delta w)}{\partial x} + z\frac{\partial(\delta \phi_x)}{\partial x} \right.$$

$$\left. - c_1 z^3 \frac{\partial^2 \delta w}{\partial x^2} - c_1 z^3 \frac{\partial(\delta \phi_x)}{\partial x} \right) dA dx dt \tag{12}$$

Using Equation (6) and performing a time integration of kinetic energy, it reads

$$\int_{t_1}^{t_2} \delta T_{Microtube} dt$$

$$= \delta \int_{t_1}^{t_2} \left(\frac{1}{2} \int_0^L \int_0^{2\pi} \left(\int_{-h/2}^{+h/2} \rho(z)(\dot{U}^2 + \dot{W}^2)dz \right) Rd\theta dx \right) dt \tag{13}$$

Velocity components of the fluid flow can be written as

$$V_x(x,t) = \dot{U} + V_f \cos\theta$$

$$V_z(x,t) = \dot{W} - V_f \sin\theta \qquad (14)$$

where $\theta = -\frac{\partial w}{\partial x}$ and V_f is the modified flow velocity using the Knudson number [31]. Using the Equation (14), the kinetic energy of the fluid flow is given as,

$$T_{Fluid} = \frac{1}{2} \int_0^L \int_{A_f} \rho_f((\dot{U} + V_f cos\theta)^2 + (\dot{W} - V_f sin\theta)^2) dA_f dx \qquad (15)$$

The Virtual work done on the flow by the curvature of the microtube includes the effects of tangential and centripetal acceleration and assuming constant density and flow velocity ($\dot{V}_f = 0$), its variation can be written as [32],

$$\delta W_{Fluid} = -I_{0f} V_f^2 \int_0^L \frac{\partial^2 w}{\partial x^2} (\sin\theta \delta u + \cos\theta \delta w)) dx \qquad (16)$$

Using the Navier-Stokes Equations, the variation of the work done by the viscous flow can be expressed as [13],

$$\delta W_{Viscosity} = -\int_0^L \left(-\mu_e A_f \frac{\partial^3 u}{\partial x^2 \partial t} - \mu_e A_f V_f \frac{\partial^3 w}{\partial x^3} sin\theta \right.$$

$$\left. + \mu_e A_f V_f \left(\frac{\partial^2 w}{\partial x^2} \right)^2 cos\theta \right) \delta U dz$$

$$-\int_0^L \left(-\mu_e A_f \frac{\partial^3 w}{\partial x^2 \partial t} - \mu_e A_f V_f \frac{\partial^3 w}{\partial x^3} cos\theta \right.$$

$$\left. - \mu_e A_f V_f \left(\frac{\partial^2 w}{\partial x^2} \right)^2 sin\theta \right) \delta W dz \qquad (17)$$

Also, variation of the virtual work done on the foundation is given by [12]:

$$\delta W_{Foundation} = \int_0^L q_e(x,t) \delta w dx$$

$$= \int_0^L (K_1 w - K_2 \nabla^4 w + K_3 w^3 + C_v \dot{w}) \delta w dx \qquad (18)$$

Including the effects of all external works δW_{ext} and using the Hamilton's principle and linearization of trigonometric terms, the governing equations, and related boundary conditions are derived.

$$\delta \int_{t_1}^{t_2} (T - U)dt + \int_{t_1}^{t_2} \delta W_{ext}dt = 0 \tag{19}$$

Based on the nonlocal Eringen elasticity theory and knowing the fact that stress in a point in the microtube is a function of the strain in other points, nonlocal stress field along *x*-direction can be expressed as [33],

$$\sigma_{xx} - e_0 a^2 \frac{\partial^2 \sigma_{xx}}{\partial x^2} = E_{11} \varepsilon_{xx} \tag{20}$$

where a is the internal characteristic length, such as the distance between atoms, e_0 is the material constant and E_{11} is the elasticity modulus. By introducing ε_{xx} from Equation (7) into Equation (20), it reads

$$\sigma_{xx} - e_0 a^2 \frac{\partial^2 \sigma_{xx}}{\partial x^2}$$
$$= E_{11}(u_{,x} + (z - z_0)\phi_{x,x} - c_1(z - z_0)^3(w_{,xx} + \phi_{x,x}) + 1/2w_{,x}^2) \tag{21}$$

After some mathematical manipulation, the nonlinear nonlocal governing equations, including the effects of fluid flow and excitation voltage of the piezoelectric, in terms of displacement coefficients can be found as

$$A_{11}\frac{\partial^2 u}{\partial x^2} + B_{11}\frac{\partial^2 \phi_x}{\partial x^2} - c_1 E_{11}\left(\frac{\partial^3 w}{\partial x^3} + \frac{\partial^2 \phi_x}{\partial x^2}\right)$$
$$+ A_{11}\frac{\partial^2 w}{\partial x^2}\frac{\partial w}{\partial x} - \left(1 - e_0 a^2 \frac{\partial^2}{\partial x^2}\right)$$
$$\times \left(I_0\ddot{u} + \hat{I}_1\ddot{\phi}_x - c_1 I_3 \frac{\partial \ddot{w}}{\partial x} - V_f I_{0f}\frac{\partial \dot{w}}{\partial x}\frac{\partial w}{\partial x} - I_{0f}V_f^2\frac{\partial^2 w}{\partial x^2}\frac{\partial w}{\partial x}\right.$$
$$\left. - \mu_e A_f \frac{\partial^3 u}{\partial x^2 \partial t} + \mu_e A_f V_f \frac{\partial^3 w}{\partial x^3}\frac{\partial w}{\partial x} + \mu_e A_f V_f \left(\frac{\partial^2 w}{\partial x^2}\right)^2\right) = 0 \tag{22}$$

$$c_1 E_{11}\frac{\partial^3 u}{\partial x^3} + c_1 F_{11}\frac{\partial^3 \phi_x}{\partial x^3} - c_1{}^2 H_{11}\left(\frac{\partial^4 w}{\partial x^4} + \frac{\partial^3 \phi_x}{\partial x^3}\right)$$

$$[4pt] \quad + c_1 E_{11} \frac{\partial^3 w}{\partial x^3} \frac{\partial w}{\partial x} + c_1 E_{11} \left(\frac{\partial^2 w}{\partial x^2} \right)^2 - \left(1 - e_0 a^2 \frac{\partial^2}{\partial x^2} \right)$$

$$\times \left[- \frac{\partial}{\partial x} \left(N_x \frac{\partial w}{\partial x} \right) + c_1 I_3 \frac{\partial \ddot{u}}{\partial x} + c_1 \bar{I}_4 \frac{\partial \ddot{\phi}_x}{\partial x} + I_0 \ddot{w} - c_1{}^2 I_6 \frac{\partial^2 \ddot{w}}{\partial x^2} \right.$$

$$- I_{0f} V_f \left(\frac{\partial \dot{u}}{\partial x} \frac{\partial w}{\partial x} + \dot{u} \frac{\partial^2 w}{\partial x^2} \right) - \hat{I}_{1f} V_f \left(\frac{\partial \dot{\phi}_x}{\partial x} \frac{\partial w}{\partial x} + \dot{\phi}_x \frac{\partial^2 w}{\partial x^2} \right)$$

$$+ 2 I_{0f} V_f \left(\frac{\partial \dot{w}}{\partial x} \right) - I_{0f} V_f \left(\dot{w} \frac{\partial^2 w}{\partial x^2} \frac{\partial w}{\partial x} \right)$$

$$- \mu_e A_f \frac{\partial^3 w}{\partial x^2 \partial t} - \mu_e A_f V_f \frac{\partial^3 w}{\partial x^3} + \mu_e A_f V_f \left(\frac{\partial^2 w}{\partial x^2} \right)^2 \frac{\partial w}{\partial x}$$

$$+ I_{0f} V_f{}^2 \frac{\partial^2 w}{\partial x^2} + \eta A V_{Piezo} \frac{\partial^2 w}{\partial x^2} + C_v \dot{w} + K_1 w$$

$$\left. - K_2 \frac{\partial^4 w}{\partial x^4} + K_3 w^3 \right] = 0 \tag{23}$$

$$B_{11} \frac{\partial^2 u}{\partial x^2} + D_{11} \frac{\partial^2 \phi_x}{\partial x^2} - c_1 \left(\frac{\partial^3 w}{\partial x^3} + \frac{\partial^2 \phi_x}{\partial x^2} \right) F_{11} + B_{11} \frac{\partial^2 w}{\partial x^2} + \frac{\partial w}{\partial x}$$

$$- c_1 E_{11} \frac{\partial^2 u}{\partial x^2} - c_1 F_{11} \frac{\partial^2 \phi_x}{\partial x^2} + c_1{}^2 \left(\frac{\partial^3 w}{\partial x^3} + \frac{\partial^2 \phi_x}{\partial^2 x} \right) H_{11}$$

$$- c_1 E_{11} \frac{\partial^2 w}{\partial x^2} \frac{\partial w}{\partial x} - \left(1 - e_0 a^2 \frac{\partial^2}{\partial x^2} \right)$$

$$+ \left(\bar{I}_1 \ddot{u} + \bar{I}_2 \ddot{\phi}_x - c_1 \bar{I}_4 \frac{\partial \ddot{w}}{\partial x} - \hat{I}_{1f} V_f \frac{\partial \dot{w}}{\partial x} \frac{\partial w}{\partial x} \right) = 0 \tag{24}$$

Here $\ddot{u}$, $\ddot{\phi}_x$ and $\ddot{w}$ are axial, rotational, and lateral accelerations. In Equations (22) to (24), the cross-sectional moments including the tube and fluid sections are given as

$$I_0 = I_{0b} + I_{0f}, \ \hat{I}_1 = I_1 - c_1 I_3, \ \hat{I}_2 = I_2 - 2c_1 I_4 + c_1^2 I_6$$

$$I_3 = I_{3b} + I_{3f}, \ \hat{I}_4 = I_4 - c_1 I_6, \ I_6 = I_{6b} + I_{6f} \tag{25}$$

To obtain the dimensionless governing equations of motion, we introduce the following transformation of the parameters and variables.

$$\hat{u} = \frac{u}{L}, \quad \hat{x} = \frac{x}{L}, \quad \hat{w} = \frac{W}{h}, \quad k_1 = \frac{L^4 K_1}{D_{11}}, \quad k_2 = \frac{K_2}{D_{11}},$$

$$k_3 = \frac{L^4 h^2 K_3}{D_{11}}, \quad e_n = \frac{e_0 a}{L}, \quad \eta = \frac{L}{R}, \quad \beta = \frac{h}{R}, \quad \rho_b = \frac{\rho_f}{\rho_{nt}},$$

$$f = \frac{A_f}{A_{nt}}, \quad V = \frac{V_f}{\omega^* L}, \quad \hat{t} = \omega^* t, \quad \mu_{eb} = \mu \sqrt{\frac{L^4}{I_{0_{nt}} D_{11}}},$$

$$C_v = \sqrt{I_{0_{nt}} D_{11}} c_v, V_{Piezo} = \frac{A_{11}^p L^2 d_{31}}{D_{11} h_p} \hat{V}_{Piezo}, \omega^* = \sqrt{\frac{D_{11}}{I_{0_{nt}} L^4}} \qquad (26)$$

Here, ω^* is the reference frequency and V is the dimensionless voltage applied. A_{11}^p is the first order axial stiffness of the piezoelectric layer, D_{11} is the total bending stiffness and d_{31} is the strain constant of piezoelectric layers. k_1, k_2 and k_3 are the linear Winkler stiffness, stiffness of the shear layer for Hetenyi foundation, and nonlinear dimensionless Winkler stiffness. e_n is the nonlocal dimensionless stress index, and η and β are dimension ratios. ρ_b, f, V and μ_{eb} are dimensionless density, the ratio of the cross-sectional area that fluid is being conveyed to the microtube's cross-sectional area, dimensionless fluid velocity, and dimensionless viscosity. For simplicity in the following equations the superscript '$-$' is dropped.

3 Boundary Condition and Approximate Solution

The Study of the nonlinear behavior of the plates and beam-like structures shows that the low-frequency modes are often dominant [34], therefore in the Galerkin approximation a couple of the first modes that satisfy boundary conditions are used to convert the coupled partial differential equations to nonlinear ordinary equations in the time domain. Considering coupling effect of the first and second modes and assuming simple supported (SS) boundary conditions, lateral displacement of the microtube can be approximated as,

$$w(x,t) = w_1(t) sin\pi x + w_2(t) sin2\pi x \qquad (27)$$

where $w_1(t)$ and $w_2(t)$ are time-dependent amplitudes of the first and second modes. As the governing equations encompass a nonlinear coupled system of

equations, similar to [35] and [36], and neglecting the effects of rotary inertia, in-plane inertia, and shear forces, an approximate solution of u and ϕ_x, for the SS microtube can be written as

$$u(x,t) = U_1(t)sin\pi x + U_2(t)sin2\pi x \tag{28}$$

$$\phi_x(x,t) = \Phi_{x_1}(t)cos\pi x + \Phi_{x_2}(t)cos2\pi x \tag{29}$$

where $U_m(t)$ and $\phi_{x_m}(t)$ for $m = 1, 2$ are corresponding axial and rotational modes. Using the shape of the first mode of vibration for the lateral displacement, Equation (27), and introducing approximate solutions for Equation (28) and Equation (29) in the governing equations of the lateral motion, Equation (24), and applying the Galerkin method, differential equation of the motion is derived as

$$\ddot{w}_1 + (\omega_1^2 + a_1V^2 + a_2V_{Piezo}^{dc} + a_2V_{Piezo}^{ac}cos\Omega t)w_1 + a_3\mu_{eb}Vw_2$$
$$+ a_4c_v\dot{w}_1 + a_5\mu_{eb}\dot{w}_1 + a_6V\dot{w}_2 + a_7w_1{}^3 + a_8w_1{}^2w_2$$
$$+ a_9w_1w_2{}^2 + a_{10}w_2{}^3 = 0$$
$$\ddot{w}_2 + b_1\mu_{eb}Vw_1 + (\omega_2^2 + b_2V^2 + b_3V_{Piezo}^{dc} + b_3V_{Piezo}^{ac}cos\Omega t)w_2$$
$$+ b_4V\dot{w}_1 + b_5\mu_{eb}\dot{w}_2 + b_6c_v\dot{w}_2 + b_7w_1{}^3 + b_8w_1{}^2w_2$$
$$+ b_9w_1w_2{}^2 + b_{10}w_2{}^3 = 0 \tag{30}$$

where ω_{n_1} is the natural frequency of the first lateral mode of the tube and ω_1 is the natural frequency of the tube including the fluid in the presence of the foundation and centripetal acceleration.

$$\omega_1 = \sqrt{\omega_{n_1}^2 + \chi_{11}V^2 + \chi_{12}k_1 + \chi_{13}k_2 + \chi_{14}\Delta T}$$

$$\omega_2 = \sqrt{\omega_{n_2}^2 + \chi_{21}V^2 + \chi_{22}k_1 + \chi_{23}k_2 + \chi_{24}\Delta T} \tag{31}$$

Equation (30) includes terms corresponding to the parametric excitation of the piezoelectric and nonlinear third-order terms from the lateral displacements related to the first and second modes. Neglecting the nonlinear terms and substituting the solution $\{w_1(t), w_2(t)\}^T = \{w_1, w_2\}^T e^{-i\omega t}$ in Equation (30), the matrix form of the linear flutter equation, including the voltage of piezoelectric, flow velocity, fluid viscosity, and damping parameter
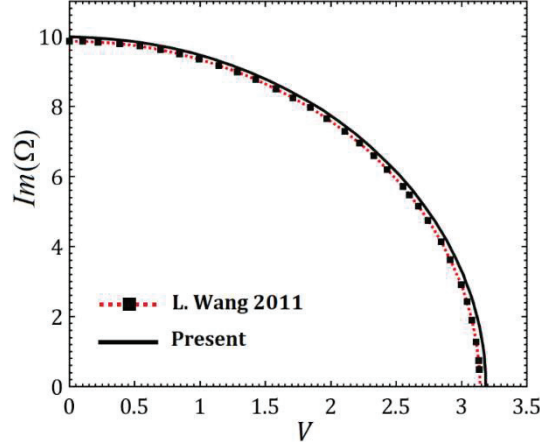
Figure 3 Comparing the results of current research for the natural frequencies related to the first mode vs. velocity with those of Ref. [24].

of the foundation, is derived as follows.

$$
\begin{bmatrix}
\omega_1^2 + a_3 V_{dc} + a_1 \mu_{eb} i\omega - \omega^2 & a_2 V i\omega + a_4 \mu_{eb} V \\
b_2 V & \omega_2^2 + b_3 V_{dc} + b_1 \mu_{eb} i\omega - \omega^2
\end{bmatrix}
\begin{bmatrix} w_1 \\ w_2 \end{bmatrix}
=
\begin{bmatrix} 0 \\ 0 \end{bmatrix}
\tag{32}
$$

4 Validation

To validate the developed method, the model is compared to the findings of [37]. For this purpose, the effect of the second mode is neglected in Equation (32) and the corresponding eigenvalue problem. Figure 3 compares the dimensionless natural frequencies related to the first mode of vibration against the flow velocity corresponding to $V_{dc} = 0$, where a very close agreement is noticeable.

5 Numerical Analysis of Two Degree of Freedom Linear Flutter

In this section, by solving the corresponding eigenvalue problem for Equation (32), the linear flutter of the microtube in different velocities is studied. The following values are used in the equations. $e_n = 0.005$, $\eta = 40$, $\beta = 0.1$, $f = 1.67$, $h/h_p = 5$, $V_{CNT}^* = 0.12$, $\eta_1 = 0.149$, $\rho_b = 0.43$, $\eta_2 = 0.934$,

$\eta_3 = 0.934$, $E_{11}^{cnt} = 5.6466$ TPa, $E_{22}^{cnt} = 7.08$ TPa, $\nu_{12}^{cnt} = 0.175$, $\rho^{cnt} = 1400$ Kg/m^3, $\nu_m = 0.34$, $E_m = 2.5$ GPa, $\rho_m = 1150$ Kg/m^3, $e_{32} = e_{31} = 17.6$ Cm^{-2}, $e_{32} = e_{31} = 17.6$ Cm^{-2}, $E_{11}^p = 63$ GPa, $\nu_p = 0.3$ and $\nu_p = 0.3$.

In Figures 4 and 5, imaginary (natural frequencies) and real components (Ω_1 and Ω_2) of eigenvalues are plotted against the flow velocity at the static dimensionless voltage of $V_{dc} = 6$. According to Figure 4, with an increase in flow velocity, characteristic curve corresponding to the first mode reaches zero at $V_A = 2.519$ and as shown in Figure 5 at this point due to the bifurcation of the real part of the characteristic curve and having a positive value, a divergence instability happens. This bifurcation is one of the characteristics of non-conservative systems. The real component of the curve stays zero up to the velocity $V_B = 5.937$ where the imaginary component approaches zero. The second mode is stable at velocities lower than V_B, where flutter divergence instability happens.

According to Figures 4 and 5, at velocities higher than V_C the first and second modes are coupled and form a flutter instability. The flow velocity at which this coupling happens is called the flutter instability limit.

Figure 6 depicts the real part of the eigenvalues corresponding to the first and second modes as a function of the flow velocity for four different static excitation voltages. As noticeable, an increase in the static excitation voltage causes the divergence and flutter instability to happen at lower velocities of the fluid flow.
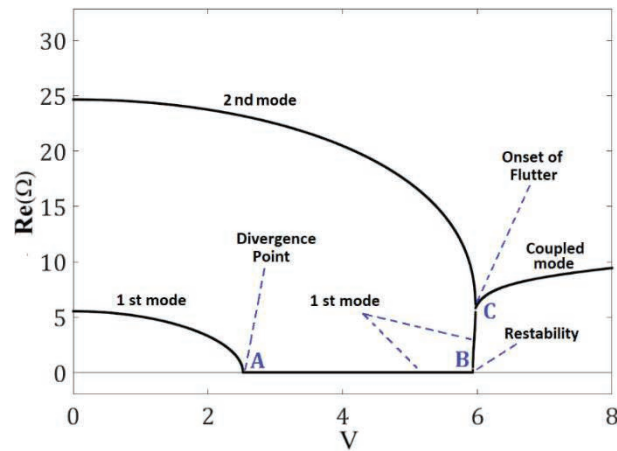

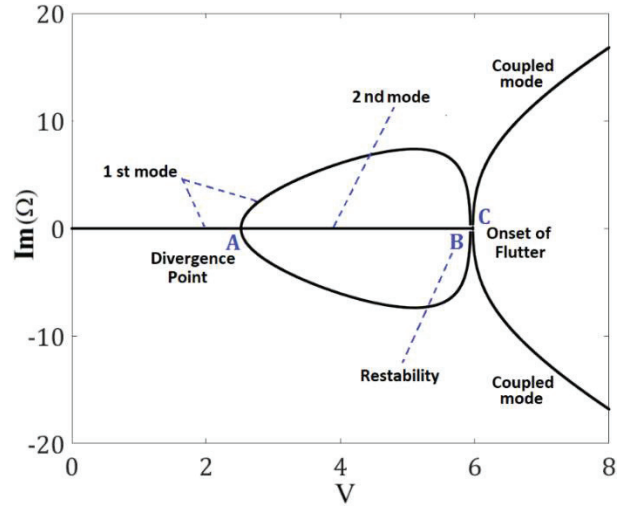**Figure 4**   Imaginary components of the eigenvalues vs flow velocity.

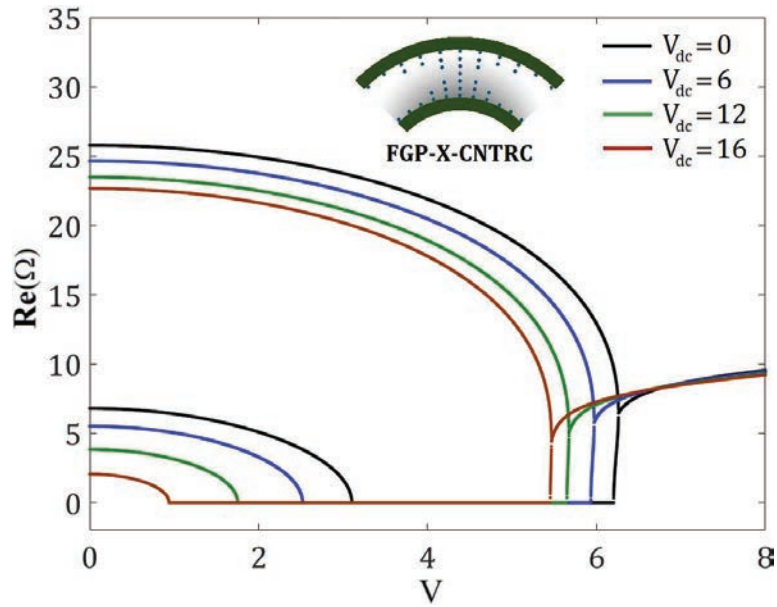**Figure 5**   Real components of the eigenvalues vs. flow velocity.

Figure 6   Real components of the eigenvalues for the first and second modal vs. flow velocity at four excitation voltages.
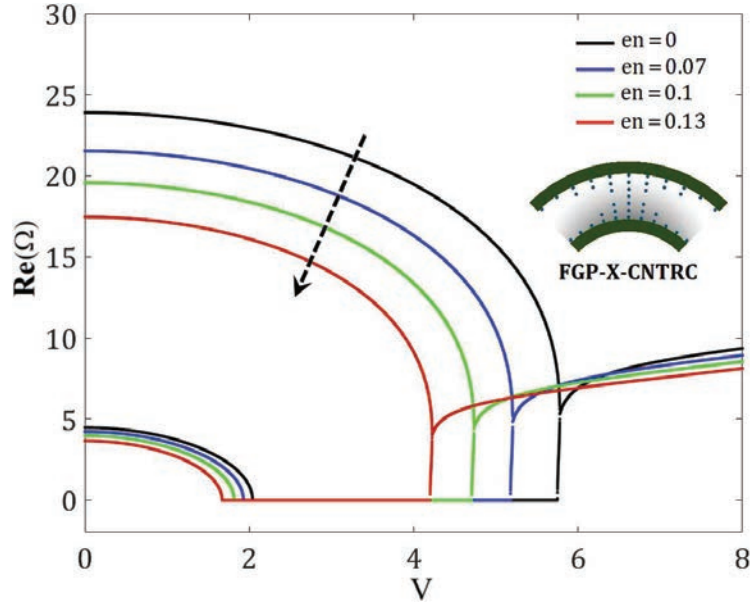
Figure 7   Real components of the eigenvalue vs. flow velocity at four nonlocal characteristic parameters (*en*).

Figure 7 shows the behavior of the real components of the eigenvalues at four different values of the nonlocal characteristic parameters. It can be observed that an increase in the *en* will shift the characteristic curves to the left and result in an earlier occurrence of divergence and flutter instability for the first and second modes.

6 Nonlinear Solution and Stability Analysis

6.1 Analysis of Nonlinear Behavior of Fluid Conveying Microtube Under Parametric Resonance

In this section, to avoid the complexity of the analysis, using the first vibrational mode, the qualitative study on the nonlinear behavior of the microtube under magnetic excitation in parametric resonance conditions is investigated. Since the solution of the nonlinear equations using the perturbation method is more accurate compared to the other common methods [38], this method was used. It is assumed that the amplitude of the excitation voltage, $V_{ac}(t)$, damping term due to viscosity of the flow, and nonlinear terms to have smaller

order of magnitude (to be weakly nonlinear) compared to the linear terms. By introducing a small dimensionless parameter, the effect of nonlinear, damping, and excitation terms are included in the first-order nonlinear perturbed solution. Using the first mode the governing perturbed Mathieu type differential equation for the lateral motion of the microtube can be written as

$$\ddot{w}_1 + \omega_1^2 w_1 = -\varepsilon\lambda_1\mu_{eb}\dot{w}_1 - \varepsilon\lambda_2 c_v\dot{w}_1 - \varepsilon\lambda_3 V_{ac}cos\Omega t w_1$$
$$- \varepsilon\lambda_4 w_1^3 - \varepsilon\lambda_5 k_3 w_1^3 \tag{33}$$

where the excitation frequency, Ω, is about two times larger compared to the fundamental frequency of the system.

To study the nonlinear behavior of the system at the foundational parametric resonance, a frequency detuning parameter, σ, is introduced to demonstrate the frequency relation as follows:

$$\Omega = 2\omega_1 + \sigma\varepsilon \tag{34}$$

To apply the method of multiple scales, the first-order approximate solution of Equation (32) is considered as:

$$w_1(t,\varepsilon) = w_{10}(T_0, T_1) + \varepsilon w_{11}(T_0, T_1), \quad T_n = \varepsilon^n t, \quad n = 0, 1 \tag{35}$$

Employing the differential operators

$$\frac{d}{dt} = D_0 + \varepsilon D_1 + \cdots , \frac{d^2}{dt^2} = D_0^2 + 2\varepsilon D_0 D_1 + \cdots , \tag{36}$$

where $D_j = \frac{\partial}{\partial T_j}$ and by substituting Equations (33) to (35) in Equation (32) and comparing the powers of ε, it reads

$$D_0^2 w_{10} + \omega_1^2 w_{10} = 0 \tag{37}$$

$$D_0^2 w_{11} + \omega_1^2 w_{11} = -\lambda_3 V_{ac} w_{10}cos\Omega T_0 - 2D_0 D_1 w_{10} + \sigma\Omega w_{10}$$
$$- \mu_{eb}\lambda_1 D_0 w_{10} - c_v\lambda_2 D_0 w_{10} - \lambda_4 w_{10}^3 - \lambda_5 k_3 w_{10}^3 \tag{38}$$

The general homogenous solution of Equation (36) is

$$w_{10}(T_0, T_1) = A_1(T_1)\, e^{i\Omega T_0/2} + \hat{A}_1(T_1)\, e^{-i\Omega T_0/2} \tag{39}$$

where $A_1(T_1)$ is an unknown complex function and $\overline{A}_1(T_1)$ is its complex conjugate. w_{11} is eliminated by introducing Equation (37) in Equation (38) as follows.

$$2I\Omega D_1 A + I\lambda_1\mu_{eb}\Omega A + I\lambda_2 c_v\Omega A - 2\sigma\Omega A$$

$$-\frac{1}{2}\lambda_3 V_{ac}\hat{A} + 6\lambda_4 A^2\hat{A} + 6\lambda_5 k_4 A^2\hat{A} = 0 \qquad (40)$$

Assuming $A_1(T_1) = x_1(T_1) + i\ x_2(T_1)$, where x_1 and x_2 are real functions, Equation (39) can be transformed into the Cartesian coordinate. In the steady-state condition, the amplitudes of the harmonic solution tend to constant values for the scaled time T_1. Therefore $\frac{dx_1}{dT_1} = 0$ and $\frac{dx_2}{dT_1} = 0$, and the equations can be derived as a set of nonlinear algebraic equations. The characteristic bifurcation curves for the frequency, velocity and voltage-response can be obtained by solving these equations using the Newton-Raphson method numerically.

6.2 Stability Analysis of Nonlinear Solutions in the Steady-State Condition

To analyze the stability of the solutions, it is assumed that x_{1s} and x_{2s} to be trivial and nontrivial steady-state solutions of the modulation equations. $x_1(T_1) = x_{1s} + x_{1p}(T_1)$ and $x_2(T_1) = x_{2s} + x_{2p}(T_1)$ where x_{1p} and x_{2p} represents the perturbed solution around the steady-state solutions. Substituting $x_1(T_1)$ and $x_2(T_1)$ into modulation equations and keeping the linear components of the equations [38], it reads

$$\dot{x}_{1p} = m_{11}x_{1p} + m_{12}x_{2p}$$

$$\dot{x}_{2p} = m_{21}x_{1p} + m_{22}x_{2p} \qquad (41)$$

where m_{ij} coefficients are

$$m_{11} = -\frac{1}{2}\lambda_1\mu_{eb} - \frac{1}{2}\lambda_2 c_v - \frac{6}{\Omega}\lambda_4 x_1 x_2 - \frac{6}{\Omega}k_3\lambda_5 x_1 x_2$$

$$m_{12} = \sigma - \frac{1}{2\Omega}\lambda_3 V_{ac} - \frac{3}{\Omega}\lambda_4 x_1^2 - \frac{9}{\Omega}\lambda_4 x_2^2 - \frac{3}{\Omega}k_3\lambda_5 x_1^2 - \frac{9}{\Omega}k_3\lambda_5 x_2^2$$

$$m_{21} = -\sigma + \frac{3}{2\Omega}\lambda_3 V_{ac} + \frac{6}{\Omega}\lambda_4 x_1^2 + \frac{3}{\Omega}\lambda_4 x_2^2 + \frac{9}{\Omega}k_3\lambda_5 x_1^2 + \frac{3}{\Omega}k_3\lambda_5 x_1^2$$

$$m_{22} = -\frac{1}{2}\lambda_1\mu_{eb} - \frac{1}{2}\lambda_2 c_v + \frac{6}{\Omega}\lambda_4 x_1 x_2 + \frac{6}{\Omega}\lambda_5 k_3 x_1 x_2 \qquad (42)$$

According to the Routh-Hurwitz stability criterion, if the real components of all the eigenvalues of the coefficient matrix $[m_{ij}]$ are negative, the nontrivial solution of the system will be stable.

7 Numerical Analysis of Nonlinear Behavior and Stability of Microtube

Fluid flow on the surface of panels and shells or through tubes results in a non-steady and nonlinear force that reduces the damping coefficient of these structures. This phenomenon results in instability and causes self-excited oscillations, which leads to fluid-induced oscillations and are called Flutter instability. In some applications, other than loads related to fluid pressure, these structures may be under the action of magnetic, electric, and thermal fields that can postpone the onset of flutter instability. Therefore, the study and identification of critical velocity corresponding to the onset of flutter instability have significant importance. On the other hand, the disturbance from the vibration of the piezoelectric induces a parametric resonance that results in lower critical velocities for the flutter instability.

7.1 Effects of System Parameters on the Amplitude of Resonance

Figure 8 shows the resonance amplitude versus the frequency tuning parameter, se, at $V = 1.5$ and $\mu_{eb} = 0.01$ corresponding to four values of excitation voltages. In this figure $\eta = \frac{L}{R} = 100$ and $\beta = \frac{h}{R} = 0.1$. It is observed that increasing excitation voltage will shift the supercritical bifurcation point of the characteristic curves to the left. In the other words, increasing the amplitude of excitation voltage will make the instability occur at lower values of the tuning parameter. On the other hand, by comparing conditions a to d, it is found that increasing the amplitude of the excitation voltage will increase the resonance amplitude and increase the width of the resonance region.

In Figure 9 characteristic bifurcation curves for four different flow velocities of $V = 0$, 2.15, 2.75, 3 are illustrated assuming $V_{ac} = 2$ and $\mu_{eb} = 0.01$. According to the figure, increasing the flow velocity will shift the bifurcation point to the left and widen the instability region. It is also noticeable that increasing the flow velocity decrease the resonance amplitude.

The frequency responses in four conditions of a) without foundation, $k_1 = 0$, and with foundation corresponding to b) $k_1 = 30$, c) $k_1 = 60$ and d) $k_1 = 90$ are shown in Figure 10. As can be seen in this figure,
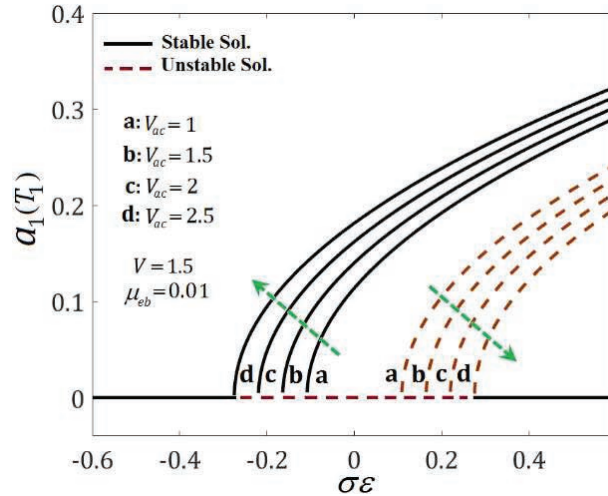
Figure 8 Resonance amplitude vs. frequency detuning parameter in the absence of the foundation for four values of the excitation amplitude.
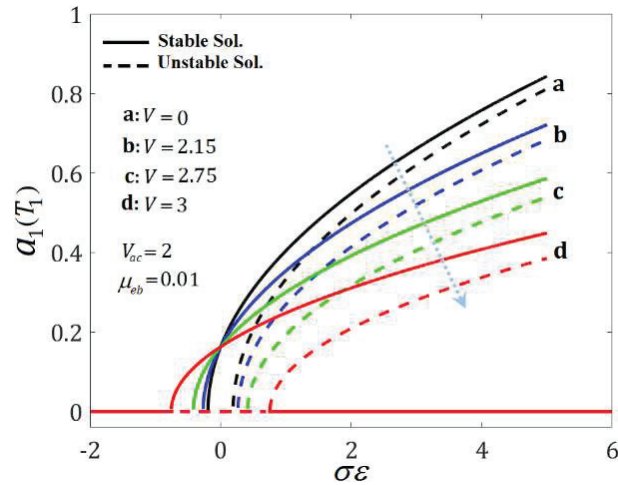

Figure 9 Resonance amplitude vs. frequency detuning parameter in the absence of the foundation for three values of the fluid flow velocity.

the presence of the foundation increases the linear stiffness and raises the curves relative to the condition without the foundation. It means that the large values of the linear stiffness have a stabilizing effect and cause the resonance amplitude to increase. Also, an increase in the linear stiffness will
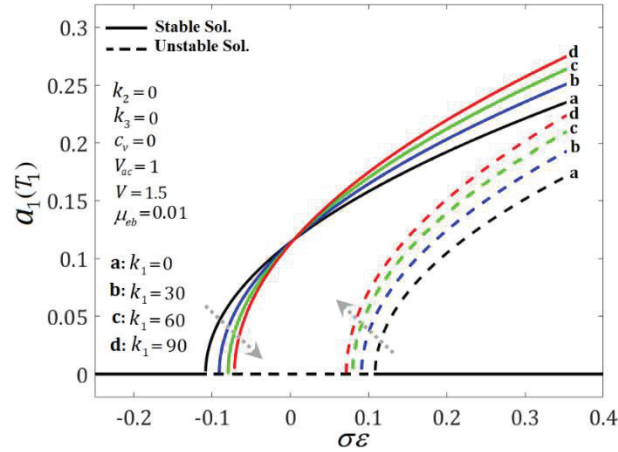
Figure 10 Comparing frequency response curves with and without the presence of the foundation for different values of linear stiffness.
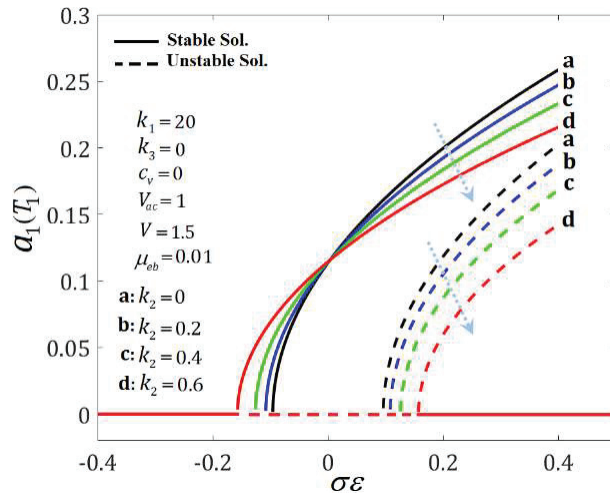

Figure 11 Comparing the frequency response for the condition with and without the shear layer of the Hetenyi foundation.

bring supercritical/subcritical points closer to each other, which results in the stability region being wider. Therefore, it can be concluded that the presence of the foundation causes delays in the occurrence of the resonance.

Figure 11 illustrates the effect of the shear layer of the Hetenyi foundation $(k_1 = k_3 = 0)$ on the characteristic curves of resonance amplitude against
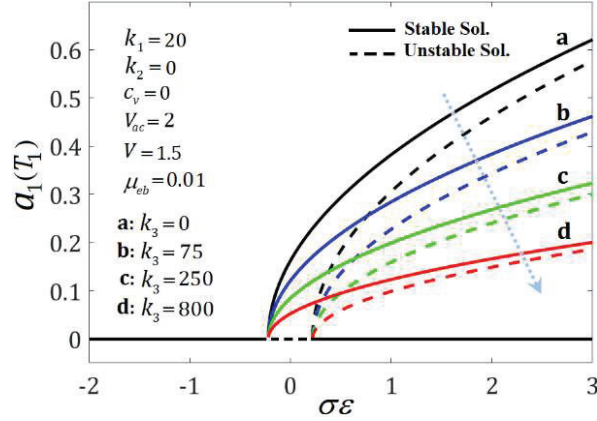
Figure 12   Comparing the frequency response of the microtube with and without nonlinear stiffness of the foundation.

detuning parameter for four different shear layer stiffness values. From Figure 11, it can be observed that an increase in the shear layer stiffness, k_2, reduces the linear behavior of the system and consequently suppresses the curves downward. On the other hand, the increase in the stiffness of the shear layer results in a decrease in the resonance amplitude and expands the resonance region. Therefore, increasing the shear layer stiffness parameter has an un-stabilizing effect on the system.

In the absence of the shear layer, $k_2 = 0$, and assuming $k_1 = 20$, Figure 12 demonstrates the effect of nonlinear foundation parameter on the frequency response curves for $V = 1.5$, $V_{ac} = 2$ and $\mu_{eb} = 0.01$. According to Figure 12, increasing the nonlinear stiffness parameter from *a* to *d* bends the curve to the right and decreases the resonance amplitude, while not affecting the width of the resonance region.

7.2 Effect of System Parameters on the Piezoelectric Resonance Amplitude

Figure 13 shows the resonance curves for different values of flow velocity, $V = 0.1$, 1.2, 1.7, 2.05, and positive value of detuning parameter, $\sigma \varepsilon = 0$. According to this figure, increasing the flow velocity will shift the supercritical/subcritical bifurcation points to the left and widen the resonance region while decreasing the resonance amplitude.

Figure 14 shows the characteristic curves of resonance amplitude against the excitation voltage in the absence of the foundation. According to this
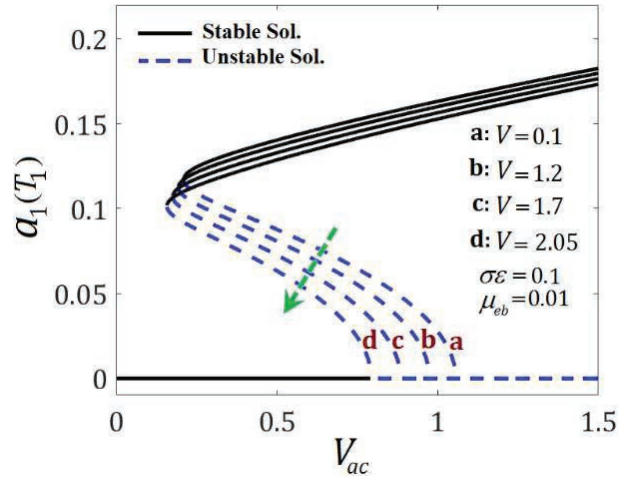
Figure 13   Resonance amplitude vs. the excitation voltage in the absence of the foundation for different velocities.
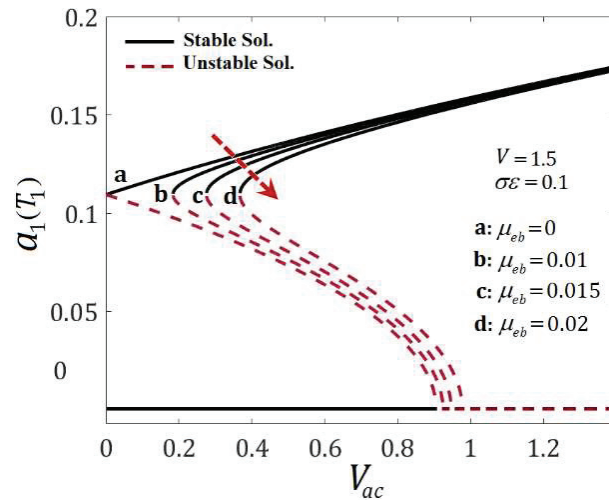

Figure 14   Characteristic curves of the resonance amplitude vs. amplitude of the excitation voltage in the absence of foundation effects for different viscosity values.

figure, increasing the dimensionless viscosity parameter, μ_{eb}, will shift the bifurcation point to the right and will reduce the amplitude and reduce the width of the resonance region. As expected, for the case of no damping effect, $\mu_{eb} = 0$, resonance will always happen.
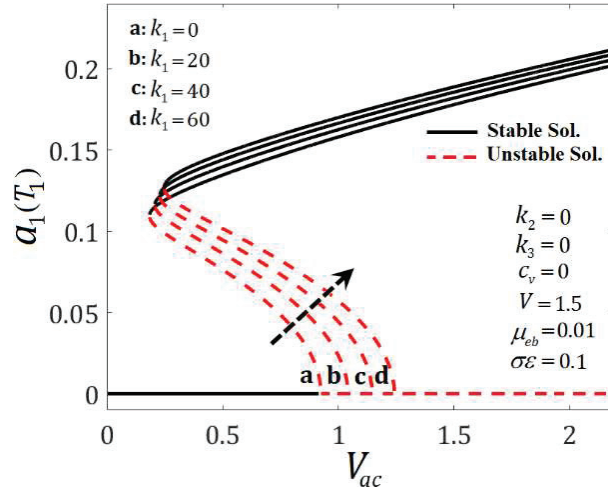
Figure 15 The frequency response in the absence/ presence of linear foundation for different stiffness values.
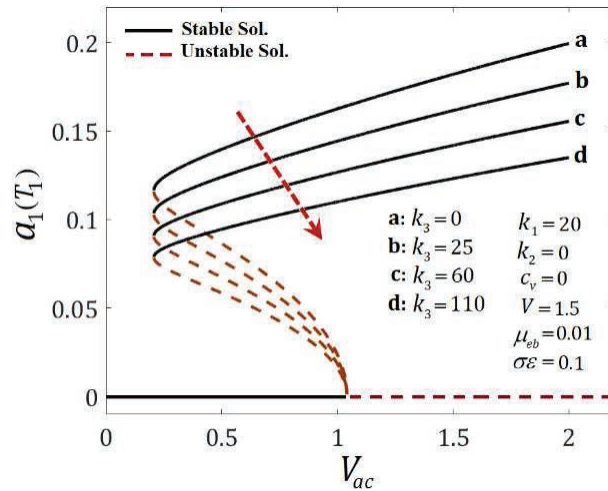

Figure 16 Piezoelectric response for four values of nonlinear stiffness parameter.

Figures 15 and 16 show the effect of linear and nonlinear stiffness parameters on the resonance curves versus the excitation voltage at four different linear and nonlinear stiffness coefficients. According to Figure 15, increasing the linear, k_1, has a stabilizing effect and shifts the bifurcation curves to the right, consequently reducing the widths of the resonance region. From
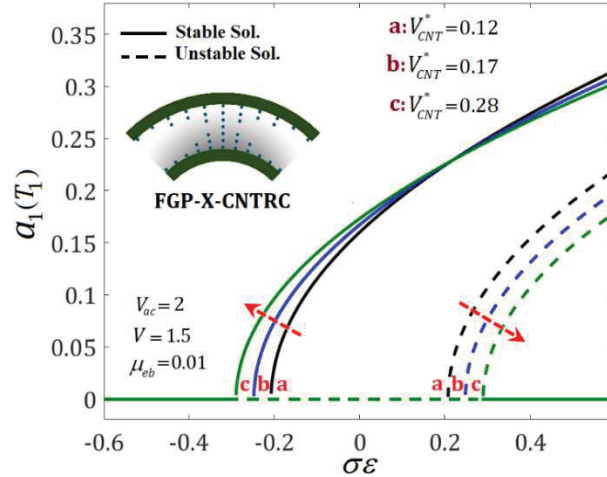
Figure 17   Comparing frequency response of microtube for three different volume fraction indexes.

Figure 16 it is noticeable that increasing the nonlinear stiffness does not affect the width of the resonance region, but as expected it increases the nonlinear softening behavior of the system and reduces the resonance amplitude.

7.3 Effect of Volume Fraction Index of Carbon nanotubes on the Frequency Response of the Microtube

In this section, the nonlinear behavior of the single-walled microtubes reinforced with carbon nanotubes with FG-X pattern is analyzed. In the absence of foundation and Considering $\mu_{eb} = 0.01$, $V_{ac} = 2$, and by fixing the dimensionless flow velocity at $V = 0.15$, the resonance amplitude of the microtube versus frequency detuning parameter, $\sigma\varepsilon$ is investigated. Figure 17 shows the resonance amplitude against frequency detuning parameter, $\sigma\varepsilon$, for three different values of the volume fraction indexes, $V_{CNT}^* = 0.12$, 0.17, 0.28. As shown, an increase in the volume fraction index of nanotubes results in a decrease in the resonance amplitude.

7.4 Effect of Temperature Loading on the Frequency and Nonlinear Response of the Microtube

To study the effects of the thermal loading on the linear flutter instability and nonlinear resonance behavior of the fluid conveying micro-tube, it is

considered that the Young modulus and thermal expansion coefficient of the matrix phase have a dependency on temperature as $E_m = (3.52 - 0.0034T)$ GPa and $\alpha_m = 45(1 + 0.0005T) \times 10^{-6}/°$K. Here $T = \Delta T + T_0$ and the reference temperature is $T_0 = 300°$ K [26]. Moreover, the micro-tube is reinforced with single-walled CNT in which its thermo-mechanical properties are considered as

$$E_{11}^{CNT}(T)[\text{TPa}] = 6.3998 - 4.338417 \times 10^{-6}\text{T}$$
$$+ 7.43 \times 10^{-6}\text{T}^2 - 4.458333 \times 10^{-6}\text{T}^3$$

$$\alpha_{11}^{CNT}(T)[10^{-6}/°\text{K}] = -1.12515 + 0.02291688\text{T}$$
$$- 2.887 \times 10^{-5}\text{T}^2 + 1.13625 \times 10^{-8}\text{T}^3 \quad (43)$$

Efficiency parameters reported by [39]: $\eta_1 = 0.137$, $\eta_2 = 1.022$, $\eta_3 = 0.715$ for the case of $V_{CNT}^* = 0.12$ were used in this study. Figure 18 shows the variation of the real part of the eigenvalues for four different temperature difference values. It can be observed that an increase in the ΔT has an un-stabilizing effect and will shift the characteristic curves to the left and will result in the earlier occurrence of divergence and flutter instability for the first and second modes.
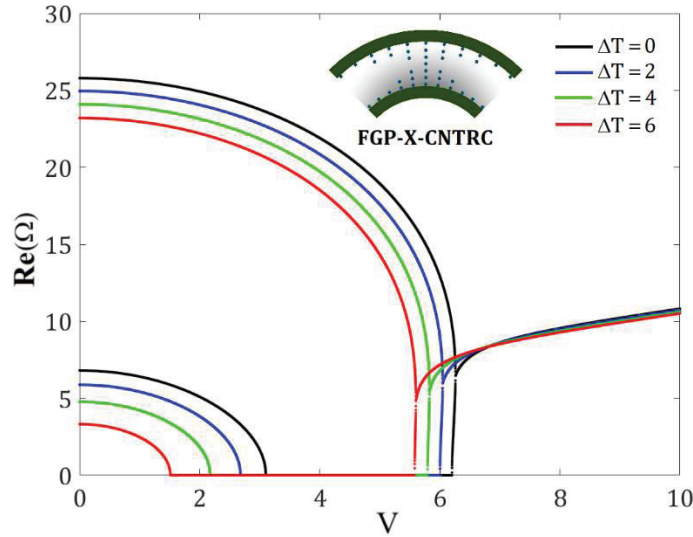

Figure 18 Variation of the real part of the eigenvalues vs. the flow velocity at four temperature differences.
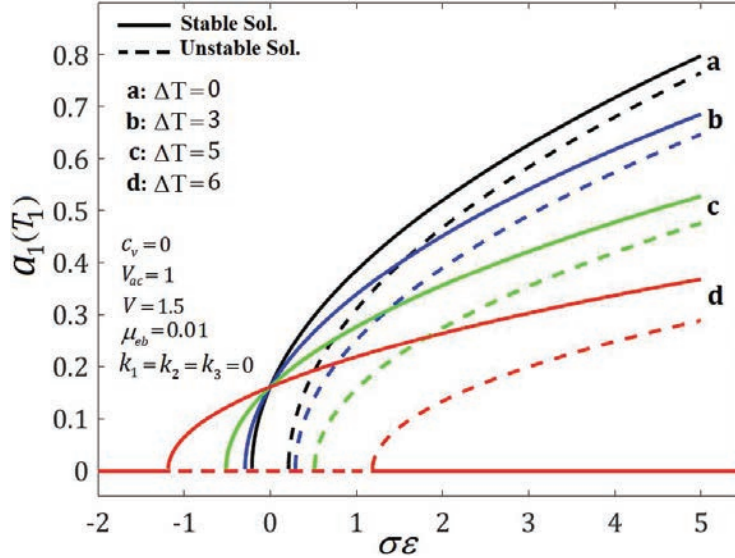
Figure 19   Comparing frequency response of the microtube at four temperature differences (ΔT).

Figure 19 illustrates the effect of the temperature difference ΔT on the frequency response of the resonance amplitude. It is noticeable that an increase in the ΔT has a softening nonlinear effect and reduces the linear behavior of the resonance amplitude and consequently suppresses the curves downward. Moreover, an increase in ΔT results in a decrease in the resonance amplitude and expands the resonance region.

8 Conclusions

In this research, nonlinear nonlocal vibrations of fluid conveying piezoelectric microtube reinforced with carbon nanotubes on a nonlinear viscoelastic foundation with the Hetenyi shear layer were studied. After deriving governing equations and using the perturbation method, modulation equations were derived and the stability of trivial and nontrivial solutions under steady conditions was studied and the effects of different parameters on the resonance amplitude was investigated. The numerical results showed that:

a. An increase in the amplitude of the excitation voltage has an unstabilizing effect and widens the resonance region.

   b. Increasing the linear stiffness has a stabilizing effect and increases the resonance amplitude and increases the linear behavior of the system and consequently postpones the occurrence of the resonance.

   c. Increasing the shear layer stiffness has an un-stabilizing effect and results in a decrease in the resonance amplitude and expands the resonance region.

   d. Increasing the nonlinear stiffness results in an increase in the softening nonlinear behavior of the system that decreases the resonance amplitude.

   e. Increasing the fluid viscosity, decreases the width of the resonance region, and increasing the fluid flow velocity widens the resonance region.

   f. Increasing the temperature difference has a softening nonlinear effect and expands the width of the resonance region.

References

[1] S. H. Mirtalebi, M. T. Ahmadian, and A. Ebrahimi-Mamaghani, "On the dynamics of micro-tubes conveying fluid on various foundations," *SN Applied Sciences*, vol. 1, no. 6, p. 547, May 2019, doi: 10.1007/s42452-019-0562-9.

[2] Y. Zhen, Y. Gong, and Y. Tang, "Nonlinear vibration analysis of a supercritical fluid-conveying pipe made of functionally graded material with initial curvature," *Composite Structures*, vol. 268, p. 113980, Jul. 2021, doi: 10.1016/j.compstruct.2021.113980.

[3] Y. Zarabimanesh, P. Roodgar Saffari, P. Roudgar Saffari, and N. Refahati, "Hygro-thermo-mechanical vibration of two vertically aligned single-walled boron nitride nanotubes conveying fluid," *Journal of Vibration and Control*, p. 10775463211006512, Mar. 2021, doi: 10.1177/10775463211006512.

[4] F. Liang, A. Gao, X.-F. Li, and W.-D. Zhu, "Nonlinear parametric vibration of spinning pipes conveying fluid with varying spinning speed and flow velocity," *Applied Mathematical Modelling*, vol. 95, pp. 320–338, Jul. 2021, doi: 10.1016/j.apm.2021.02.007.

[5] P. Roodgar Saffari, M. Fakhraie, and M. A. Roudbari, "Size-Dependent Vibration Problem of Two Vertically-Aligned Single-Walled Boron Nitride Nanotubes Conveying Fluid in Thermal Environment Via Nonlocal Strain Gradient Shell Model," *Journal of Solid Mechanics*, vol. 13, no. 2, pp. 164–185, 2021, doi: 10.22034/jsm.2020.1895313.1561.

[6] P. R. Saffari, M. Fakhraie, and M. A. Roudbari, "Nonlinear vibration of fluid conveying cantilever nanotube resting on visco-pasternak foundation using non-local strain gradient theory," *Micro & Nano Letters*, vol. 15, no. 3, pp. 181–186, Mar. 2020, doi: 10.1049/mnl.2019.0420.

[7] B. Zhu, Q. Xu, M. Li, and Y. Li, "Nonlinear free and forced vibrations of porous functionally graded pipes conveying fluid and resting on nonlinear elastic foundation," *Composite Structures*, vol. 252, p. 112672, Nov. 2020, doi: 10.1016/j.compstruct.2020.112672.

[8] R. W. Gregory and M. P. Paidoussis, "Unstable oscillation of tubular cantilevers conveying fluid II. Experiments," *Proceedings of the Royal Society of London. Series A. Mathematical and Physical Sciences*, vol. 293, no. 1435, pp. 528–542, 1966.

[9] M. P. Paidoussis, *Fluid-structure interactions: slender structures and axial flow*, vol. 1. Academic press, 1998.

[10] J. K. Sinha, S. Singh, and A. R. Rao, "Finite element simulation of dynamic behaviour of open-ended cantilever pipe conveying fluid," *Journal of sound and vibration*, vol. 1, no. 240, pp. 189–194, 2001.

[11] R. Ansari, R. Gholami, and A. Norouzzadeh, "Size-dependent thermo-mechanical vibration and instability of conveying fluid functionally graded nanoshells based on Mindlin's strain gradient theory," *Thin-Walled Structures*, vol. 105, pp. 172–184, 2016.

[12] R. Ansari, R. Gholami, A. Norouzzadeh, and S. Sahmani, "Size-dependent vibration and instability of fluid-conveying functionally graded microshells based on the modified couple stress theory," *Microfluidics and nanofluidics*, vol. 19, no. 3, pp. 509–522, 2015.

[13] R. Ansari, A. Norouzzadeh, R. Gholami, M. F. Shojaei, and M. A. Darabi, "Geometrically nonlinear free vibration and instability of fluid-conveying nanoscale pipes including surface stress effects," *Microfluidics and nanofluidics*, vol. 20, no. 1, p. 28, 2016.

[14] M. Şimşek, "Nonlinear free vibration of a functionally graded nanobeam using nonlocal strain gradient theory and a novel Hamiltonian approach," *International Journal of Engineering Science*, vol. 105, pp. 12–27, Aug. 2016, doi: 10.1016/j.ijengsci.2016.04.013.

[15] A. Marzani, M. Mazzotti, E. Viola, P. Vittori, and I. Elishakoff, "FEM formulation for dynamic instability of fluid-conveying pipe on nonuniform elastic foundation," *Mechanics based design of structures and machines*, vol. 40, no. 1, pp. 83–95, 2012.

[16] X. Yang, T. Yang, and J. Jin, "Dynamic stability of a beam-model viscoelastic pipe for conveying pulsative fluid," *Acta Mechanica Solida Sinica*, vol. 20, no. 4, pp. 350–356, 2007.

[17] H. Liu, Z. Lv, and H. Tang, "Nonlinear vibration and instability of functionally graded nanopipes with initial imperfection conveying fluid," *Applied Mathematical Modelling*, vol. 76, pp. 133–150, Dec. 2019, doi: 10.1016/j.apm.2019.06.011.

[18] Z.-Q. Lu, K.-K. Zhang, H. Ding, and L.-Q. Chen, "Nonlinear vibration effects on the fatigue life of fluid-conveying pipes composed of axially functionally graded materials," *Nonlinear Dynamics*, vol. 100, no. 2, pp. 1091–1104, Apr. 2020, doi: 10.1007/s11071-020-05577-8.

[19] K. Zhou, Q. Ni, L. Wang, and H. L. Dai, "Planar and non-planar vibrations of a fluid-conveying cantilevered pipe subjected to axial base excitation," *Nonlinear Dynamics*, vol. 99, no. 4, pp. 2527–2549, Mar. 2020, doi: 10.1007/s11071-020-05474-0.

[20] H. Ding, J. Ji, and L.-Q. Chen, "Nonlinear vibration isolation for fluid-conveying pipes using quasi-zero stiffness characteristics," *Mechanical Systems and Signal Processing*, vol. 121, pp. 675–688, Apr. 2019, doi: 10.1016/j.ymssp.2018.11.057.

[21] L. Wang and Q. Ni, "On vibration and instability of carbon nanotubes conveying fluid," *Computational Materials Science*, vol. 43, no. 2, pp. 399–402, 2008.

[22] T. P. Chang, "Thermal-mechanical vibration and instability of a fluid-conveying single-walled carbon nanotube embedded in an elastic medium based on nonlocal elasticity theory," *Applied Mathematical Modelling*, vol. 36, no. 5, pp. 1964–1973, 2012.

[23] M. Rafiee, J. Yang, and S. Kitipornchai, "Thermal bifurcation buckling of piezoelectric carbon nanotube reinforced composite beams," *Computers & Mathematics with Applications*, vol. 66, no. 7, pp. 1147–1160, 2013.

[24] M. Rasekh and S. E. Khadem, "Nonlinear vibration and stability analysis of axially loaded embedded carbon nanotubes conveying fluid," *Journal of Physics D: Applied Physics*, vol. 42, no. 13, p. 135112, 2009.

[25] J. H. Yang, J. Yang, and S. Kitipornchai, "Nonlinear dynamic response of electro-thermo-mechanically loaded piezoelectric cylindrical shell reinforced with BNNTs," *Smart Materials and Structures*, vol. 21, no. 12, p. 125005, 2012.

[26] A. Alibeigloo, "Free vibration analysis of functionally graded carbon nanotube-reinforced composite cylindrical panel embedded in piezo-electric layers by using theory of elasticity," *European Journal of Mechanics-A/Solids*, vol. 44, pp. 104–115, 2014.

[27] M. Mohammadimehr and M. Mahmudian-Najafabadi, "Bending and free vibration analysis of nonlocal functionally graded nanocomposite Timoshenko beam model rreinforced by SWBNNT based on modified coupled stress theory," *Journal of Nanostructures*, vol. 3, no. 4, pp. 483–492, 2013.

[28] M. Mohammadimehr, M. Salemi, and B. R. Navi, "Bending, buckling, and free vibration analysis of MSGT microcomposite Reddy plate reinforced by FG-SWCNTs with temperature-dependent material properties under hydro-thermo-mechanical loadings using DQM," *Composite Structures*, vol. 138, pp. 361–380, 2016.

[29] H. Zhang et al., "Analysis of functionally graded carbon nanotube-reinforced composite structures: A review," *Nanotechnology Reviews*, vol. 9, pp. 1408–1426, Dec. 2020, doi: 10.1515/ntrev-2020-0110.

[30] A. H. Nayfeh and D. T. Mook, *Nonlinear oscillations*. John Wiley & Sons, 2008.

[31] A. Ghorbanpour Arani, E. Haghparast, and Z. Khoddami Maraghi, "Vibration analysis of double bonded composite pipe reinforced by BNNTs conveying oil," *Journal of Computational Applied Mechanics*, vol. 46, no. 2, pp. 93–105, 2015, doi: 10.22059/jcamech.2015.55092.

[32] P. Zhu and K. M. Liew, "Free vibration analysis of moderately thick functionally graded plates by local Kriging meshless method," *Composite Structures*, vol. 93, no. 11, pp. 2925–2944, 2011.

[33] A. C. Eringen, "On differential equations of nonlocal elasticity and solutions of screw dislocation and surface waves," *Journal of applied physics*, vol. 54, no. 9, pp. 4703–4710, 1983.

[34] W. Zhang, J. Yang, and Y. Hao, "Chaotic vibrations of an orthotropic FGM rectangular plate based on third-order shear deformation theory," *Nonlinear Dynamics*, vol. 59, no. 4, pp. 619–660, 2010.

[35] M. Amabili and S. Farhadi, "Shear deformable versus classical theories for nonlinear vibrations of rectangular isotropic and laminated composite plates," *Journal of sound and vibration*, vol. 320, no. 3, pp. 649–667, 2009.

[36] Y. Fu and J. Ruan, "Nonlinear active control of damaged piezoelectric smart laminated plates and damage detection," *Applied Mathematics and Mechanics*, vol. 29, no. 4, pp. 421–436, 2008.

[37] L. Wang, "A modified nonlocal beam model for vibration and stability of nanotubes conveying fluid," *Physica E: Low-dimensional Systems and Nanostructures*, vol. 44, no. 1, pp. 25–28, 2011.

[38] X. Y. Guo, W. Zhang, and M. Yao, "Nonlinear dynamics of angle-ply composite laminated thin plate with third-order shear deformation," *Science China Technological Sciences*, vol. 53, no. 3, pp. 612–622, 2010.

[39] M. Mirzaei and Y. Kiani, "Thermal Buckling of Temperature Dependent FG-CNT Reinforced Composite Plates," *Meccanica*, vol. 51, pp. 2185–2201, Sep. 2016, doi: 10.1007/s11012-015-0348-0.

Biographies

Mehdi Azhdarzadeh received his PhD in Mechanical Engineering from the University of Alberta, Canada. His research interests are aerosol and particle engineering, water treatment, robotics, controls, and mechanical modeling.

Reza Jahangiri received his BSc, MSc, and PhD degree in mechanical engineering from the Urmia, Sharif University of Technology, and the University of Tabriz, respectively, Iran. After getting his PhD, he joined the faculty of engineering of Azad University, IRAN, where he is an assistant professor in the Mechanical Engineering Department. His current research interests

are in the areas of fluid-induced nonlinear and chaotic magneto-piezo-aero-thermo_elastic behavior of the Beams/Plates/Shells using elasticity theories. Also, he is working in the field of nonlinear robust/fuzzy control and nano/microfluidic.

Akbar Allahverdizadeh teaches in the Department of Mechatronics Engineering at the University of Tabriz, Iran. He received his Bachelor's degree in Mechanical Engineering from the Isfahan University of Technology, Iran in 2000 and his Master's and Doctoral degrees in Mechanical Engineering from the University of Tehran, Iran in 2006 and 2013. His research interests are in the areas of mechatronics, biomechanics, and vibration control.

Behnam Dadashzadeh is an assistant professor of mechatronics engineering at the University of Tabriz since 2013. He received his BSc from the University of Tabriz in 2005 and his MSc and PhD from the University of Tehran in 2007 and 2013, all in Mechanical Engineering. His research interests include dynamics and control of biped robots running and walking, mechatronic systems, mobile robots, and musculoskeletal biomechanics. He has international research experiences at the University of Calgary working on event-based

control of bipedal running in 2012, at the Oregon State University working on modeling and control of ATRIAS in 2013, and at École Nationale d'ingénieurs de Tarbes working on actuation systems for robotic hands.

Ramin Nabati received his MSc in mechanical engineering from Azad University. His research interest is microfluidic.